Reprinted from

Thomas J. Schmugge Jean-Claude André
Editors

Land Surface Evaporation

Measurement and Parameterization

Springer-Verlag
New York Berlin Heidelberg London
Paris Tokyo Hong Kong Barcelona

9
Fluxes in the Surface Layer Under Advective Conditions

H.A.R. de Bruin, N.J. Bink, and L.J.M. Kroon

1. Introduction

The surface fluxes of water vapor, sensible heat, and momentum are important in many meteorological, agricultural, and hydrological problems. In most applications it is (tacitly) assumed that the Earth's surface is, on the scale of interest, horizontally homogeneous. An example is the way in which the surface fluxes are parameterized in models for the prediction of weather and climate. Also, most measuring techniques used for the determination of the surface fluxes are based on the assumption of horizontal homogeneity.

Although the last word on the uniform case has certainly not been said, for most practical calculations the Monin-Obukhov similarity theory (Panofsky and Dutton 1984; Brutsaert 1982) provides a suitable description of the surface fluxes. Reliable estimates can be obtained from the vertical profiles of temperature, humidity, and wind speed or, alternatively, the variances of these quantities.

In reality the Earth's surface is seldom homogeneous, and even if a surface is uniform, the meteorological conditions are often such that horizontal differences exist. Examples are partly clouded skies or surfaces partly wetted by rain. Matters become much more complicated in the heterogeneous case, even if we exclude hilly or mountainous terrains. Several types of nonuniform surfaces can be distinguished, primarily depending on the scale being considered. For meteorological models the horizontal scale varies between, say, 10 km (mesoscale models) and 300 km (general circulation models). In agriculture the scale of interest is about 100 m to 1 km, while hydrologists deal with scales of 1 km to 100 km depending on the size of the watershed.

Small scale irregularities at the surface will affect only the atmospheric surface layer (ASL), but irregularities of the order of 10–50 km also influence the planetary boundary layer (PBL), while larger ones can affect the flow of the free atmosphere.

In this chapter we will consider only a surface that is nonuniform on a small scale; so only the atmospheric surface layer is affected. For this relatively simple case we distinguish two types of nonuniform surfaces:

Type a: A nonuniform terrain with a constant surface roughness, but different thermal properties described in the previous chapter as the Oasis effect. In this case, primarily the fluxes of heat and water vapor are affected by the irregularities and not the momentum flux. An example will be considered in this chapter.

Type b: A uniform terrain covered with isolated obstacles. Then, the momentum flux is affected, while the sensible and latent heat fluxes are hardly disturbed. An example is the typical Dutch landscape of meadows, where cows, measuring vans, isolated trees, and ditches are the obstacles.

Here we will consider an example of type a, viz. an irrigated grassland field, surrounded by dry land covered with a vegetation of about equal height. This field is located in the area of "La Crau" in the South of France, where the Mistral (i.e., a strong dry northerly wind) frequently blows. Some first results are shown from a field experiment car-

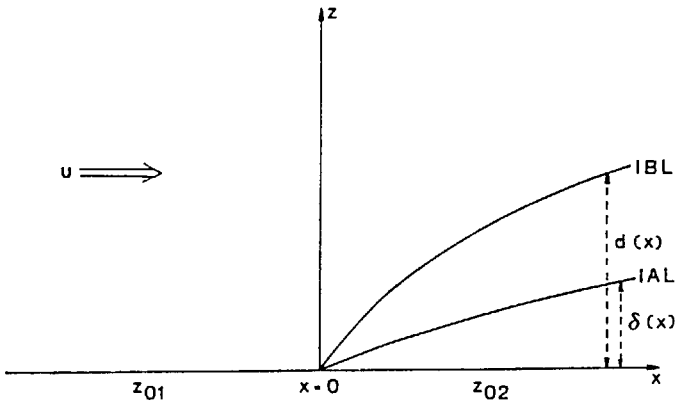

FIGURE 9.1. Definition sketch of a change in surface conditions.

ried out in June 1987. The turbulent fluxes of heat, water vapor, and momentum were measured with the eddy-correlation technique over the dry uniform upwind terrain and at several heights over the irrigated field downwind from a sudden step change in surface conditions. Also the vertical profiles of temperature, humidity, and wind speed were observed at different distances from the leading edge. It appears that the observed profiles are fairly well described by the second-order closure model of Rao et al. (1974). A first analysis of the collected data reveals that in the case where the Mistral occurs the fluxes of heat and water vapor over the irrigated field vary considerably with height in the first 15 m. Furthermore, it appears that the profiles of temperature and humidity change with the distance from the leading edge. Also, the applicability of the Monin–Obukhov similarity theory is considered. For this purpose, the fluxes are calculated with the variance technique (Tillman, 1972). Large deviations with observation above the irrigated field are found, but evidence is given that the variance method still can be applied to this surface type for water vapor.

Results for this field will be compared with those obtained earlier from a type b site in the Netherlands. Also results will be used from measurements over the dry land that surrounds the irrigated grassland. The dry area is an extensive uniform terrain.

It is noted that data of fluxes near the surface under advective conditions are rather scarce. Lang et al. (1983) did measurements in Australia above in irrigated rice field, thus also a type a field. These authors considered the differences between the exchange coefficients for heat and water vapor.

2. Theory

2.1 General

In most models that describe the structure of the turbulent flow over a sudden step-change in surface conditions, the region of the atmosphere affected by the step-change is referred to as the internal boundary layer (IBL). Furthermore, it is assumed that the flow in the lower portion of the IBL is locally adapted to the new surface conditions. This sublayer is called the internal adapted layer (IAL) (Kroon, 1985) or internal equilibrium sublayer (Brutsaert, 1982). Note that the surface fluxes within this adapted layer vary with the distance from the step change. The depth of the IBL and IAL, whose absolute value depends on their definition, grows with the distance, x, downwind from the step-change (Fig. 9.1).

Reviews of existing models dealing with this issue are given by Brutsaert (1982) and Kroon (1985). The majority of these models deal with a step-change in surface roughness and consider the behavior of the wind field and momentum flux only. It is concluded in both reviews that the second-order closure approach proposed by Rao et al. (1974) is the most promising. In Appendix 2 a brief description of this approach is given. Some applications of the model of Rao et al. (1974) will be presented in this chapter.

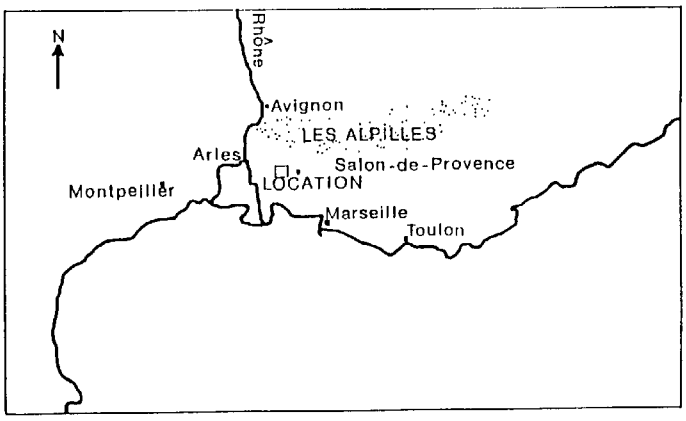

FIGURE 9.2. The location of the Crau experiment, part of the EC program "regional parameterization of the surface fluxes."

A drawback of this approach is that al first- and second-order moments such as $\overline{w'q'}$, $\overline{u'w'}$, $\overline{u'q'}$ etc. must be specified at the surface both upwind and downwind from the discontinuity at $x=0$. Rao et al. (1974) assumed that at the surface the relative humidity is a constant after the step-change. This is unrealistic (Brutsaert, 1982). For this reason we introduced the "big leaf" concept of Monteith (1981) as a lower boundary condition in the model.

2.2 Variance Method

To illustrate how a sudden dry-to-wet step-change at the surface affects the fluxes of heat and water vapor, we will consider the so-called "variance method." This method is based on the Monin-Obukhov similarity theory. For horizontally uniform surfaces it predicts that

$$\frac{\sigma_T}{|\theta_*|} = f\left(\frac{z}{L}\right) \tag{9.1}$$

For the explanation of the symbols see Appendix 1. Tillman (1972) has proposed:

$$\frac{\sigma_T}{\theta_*} = C_1\left(C_2 - \frac{z}{L}\right)^{-1/3} \qquad (L < 0) \tag{9.2}$$

This leads to

$$H = \rho c_p\left(\frac{\sigma_T}{C_1}\right)^{3/2}\left(\frac{kgz}{\theta}\right)^{1/2}\left(\frac{C_2 - z/L}{-z/L}\right)^{1/2} \qquad (L<0) \tag{9.3}$$

According to Equation (9.3) (C_2=0.05) for $z/L < -0.1$ the so-called free convection limit is reached, and H is approximately given by

$$H = \rho c_p\left(\frac{\sigma_T}{C_1}\right)^{3/2}\left(\frac{kgz}{\theta}\right)^{1/2} \tag{9.4}$$

In that case Equation (9.1) reads (Wyngaard et al., 1971)

$$\frac{\sigma_T}{|\theta_*|} = C_1\left(-\frac{z}{L}\right)^{-1/3} \tag{9.5}$$

This expression is very convenient for practical applications since it requires one fast responding thermometer only. Since, in most cases, H is relatively small if $z/L > -0.1$ this implies that H is primarily determined by σ_T while u_* plays a less important role. If this picture is correct, one expects that Equations (9.3) and (9.4) will be applicable for surfaces over which the temperature is not disturbed, whereas deviations of these equations must be expected in the case of the dry-to-wet transition we are considering.

3. Experimental Set-up and Data Processing

In June 1987 an experiment was carried out in which we studied the airflow over an extreme change of terrain conditions from a desert-like terrain to (occasionally) irrigated grass. The (local) surface roughness, z_0, of the dry terrain was about 0.01 m and the surface roughness of the grass terrain varied from 0.03 m at the beginning of the measurement period to 0.06 m at the end. The location was about 10 km east of Salon-de-Provence at Mas Capelan, France at 43.38°N and 4.59°E in the Crau plain (Fig. 9.2).

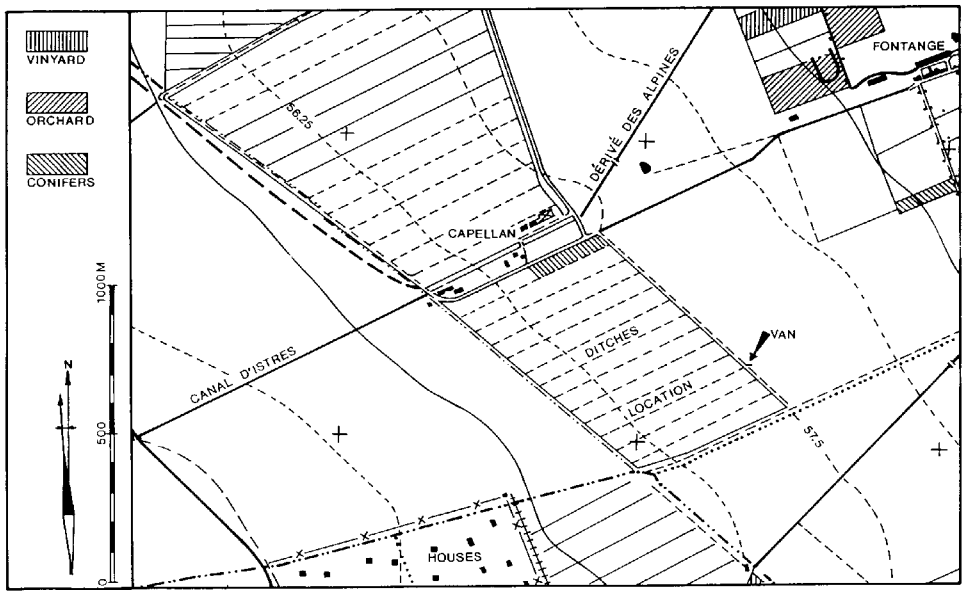

FIGURE 9.3. The experimental site and its direct surroundings.

The alluvial plain extends for 50,000 ha with the Rhone at its west side, the Alpilles mountains in the north, and the Mediterranean in the south. The experimental site (Fig. 9.3) was located on the border of the Petite or Wet Crau and the Grande or Dry Crau. The Petite Crau is mainly covered with orchards and fields with all kinds of crops, most of them surrounded by wind breaks. The Grande Crau is a stone desert covered with some herbs and isolated, low shrubs. At the northwest end of the

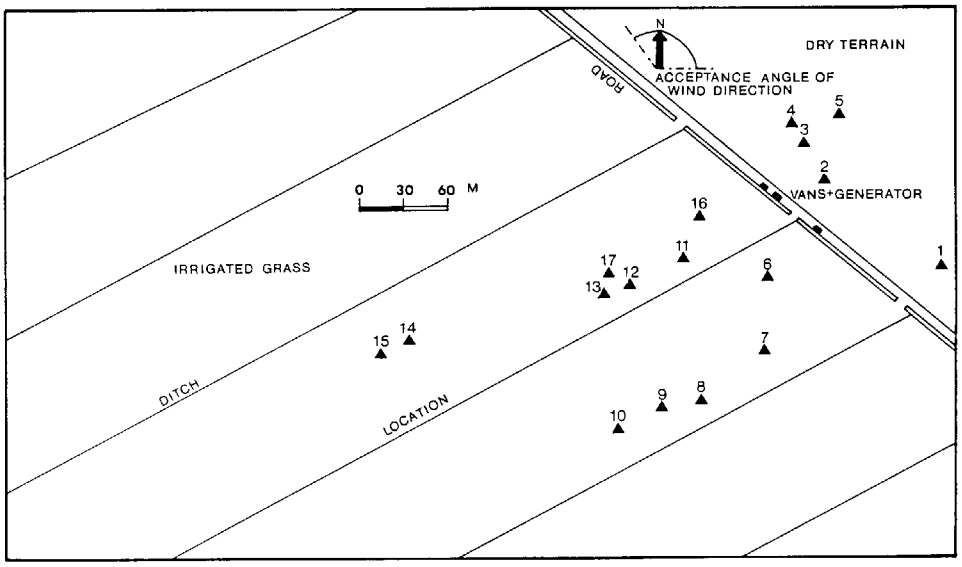

FIGURE 9.4. The experimental setup at La Crau, June 1987, of the Agricultural University Wageningen and the Free University of Amsterdam.

experimental site a small windbreak is present. The fetch for the dry terrain was at least 1 km.

In Table 9.1 and Figure 9.4 an overview of the experimental setup is given.

At no. 4 (Fig. 9.4), above the dry terrain a Kaijo–Denki one-component sonic anemometer, a Lyman-α humidity sensor and thermocouple were mounted at 6.10 m height. At the locations 8, 9, and 10 above the grass terrain at three different heights, 4.1, 6.7, and 13.0 m, three-component sonic anemometers (Kaijo–Denki) and Lyman-αs humidity fluctuation meters were installed. Fast responding thermocouples were mounted at the 4 and 6 m level.

The Lyman-αs are "self-build" except for the source and the detector; these are constructed by Glass Technologists, Maryland. The Lyman-αs were positioned downwind of the sonics and the separation between the w-sensor and the Lyman-α was 0.5 m (1 m at the 13 m level); all other components were nearer.

Corrections of the eddy correlation data due to distortion have not yet been applied. These errors can be significant, but do not affect our results, except those shown in Fig. 9.12, this is partly due to the fact that the relation between σ_T/Θ^* and z/L is not very sensitive to these distortion errors.

The profile measurements were carried out using shielded and aspirated psychrometers for temperature and humidity measurements and cup anemometers for the windprofiles. In the 10 m masts (11 and 12 in Fig. 9.4) psychrometers with Pt-100 resistance sensors are used (precision: 0.1 °C for the dry bulb temperature and 0.5 g/m³ for the humidity). The small cup anemometers have a mean starting speed of 0.2 m/s and the first-order response length is 0.9 m. The psychrometers have been calibrated both in the laboratory (absolute calibration of the Pt-100s) and the field (relative calibration of the psychrometer as a whole). The cup anemometers are calibrated in a wind tunnel. These instruments are self-developed and constructed at our laboratory.

In the 24 m masts the equipment of the department of Meteorology of the Free University of Amsterdam was installed (Vugts et al., 1988).

The turbulence signals were sampled at a rate of 10 Hz and 1 Hz was used for the profile measurements. All samples are written on magnetic tape. The sampling process was controlled with a PDP 11-24 minicomputer installed in a measuring van. The data-processing software allows us to collect samples digitally up to a total of 2000 Hz from a maximum of 200 channels. The system accepts analogue and digital signals. The frequency and the electrical range are separately adjustable for each channel such that the resolution is optimal and the natural range to be expected is covered. The frequency response of all the instruments used for the turbulence measurements ranges from at least 5 to 0.001 Hz. Within this range more than 95% of the flux-carrying fluctuations are covered (McBean and Miyake, 1972).

The data were further processed with the aid of a PDP 11-44 computer at the laboratory. The sampled signals were reduced to 30 min averages. The standard deviation and relevant correlation products of the signal with and without the removal of a linear trend were calculated. The

TABLE 9.1. The instruments.

Dry terrain
1. Psychrometers and cup anemometers at 3 and 0.75 m
2. Stevenson screen (thermohygrograph, minimum and maximum temperature
3. Net pyrradiometer and Heimann KT24 infrared-radiation thermometer (surface temperature)
4. Eddy correlation equipment at 6.10 m (1-component sonic, thermocouple, and Lyman-α humidity-fluctuation meter)
5. Net pyrradiometer and soil heat flux plates (2)
Wet terrain
6. Net pyrradiometer and soil heat flux plates (2×)
7. Net pyrradiometer, Stevenson screen
8. Eddy correlation equipment at 6.7 m (3-component sonic, Lyman-α thermocouple)
9. Cup anemometers (24, 18, 12, 6, 3, 1.5, 0.75 m); psychrometers (24, 12, 6, 3, 0.75 m); Eddy correlation equipment at 13 m (3-component sonic and Lyman-α)
10. Eddy correlation equipment (see 8) at 4.1 m
11. Cup anemometers (10, 7.5, 5, 3, 2, 1.5, 1, 0.75, 0.5, 0.25 m); psychrometers (10, 5, 3, 2, 1, 0.5) m
12. As 11
13. Net pyrradiometer and Heimann KT24 infrared-radiation thermometer (surface temperature)
14. Cup anemometers (24, 18, 12, 6, 3, 1.5, 0.75 m); psychrometers (24, 12, 6, 3, 0.75 m)
15. Stevenson screen
16. Soil heat flux plate and soil temperature (−2, −10, −25, −50 cm) with PT-100 resistance thermometers
17. Soil heat flux plate and soil temperature (−2, −10, −25, −50 cm) with PT-100 resistance thermometers

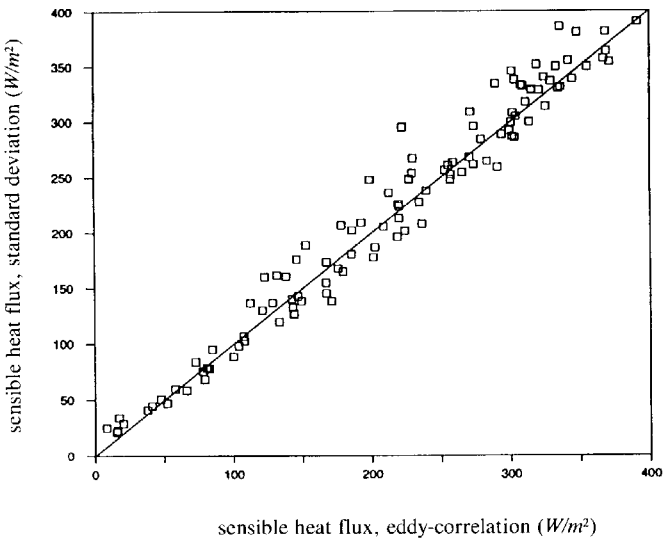

FIGURE 9.5. Uniform terrain. The sensible heat flux measured with the eddy-correlation method at location 4 (Fig. 9.4) compared with the sensible heat flux calculated with the variance technique.

reduced signals were converted to obtain engineering values. All raw data are also stored on tape.

The heat flux at 13 m is calculated from the sonic temperature using the method proposed by Schotanus et al. (1983) since no thermocouple was installed at that height. The same procedure is also adopted to calculate other products like σ_T and $\overline{Tq'}$ at the 13 m level. The method could be checked with the measurements at 4 and 6 m and provides accurate results.

The friction velocity, necessary for Equation (9.3), at the dry terrain for z/L negative is obtained from (Panofsky and Dutton, 1984)

$$\frac{\sigma_w}{u_*} = 1.25\left(1 - 3\frac{z}{L}\right)^{1/3} \tag{9.6}$$

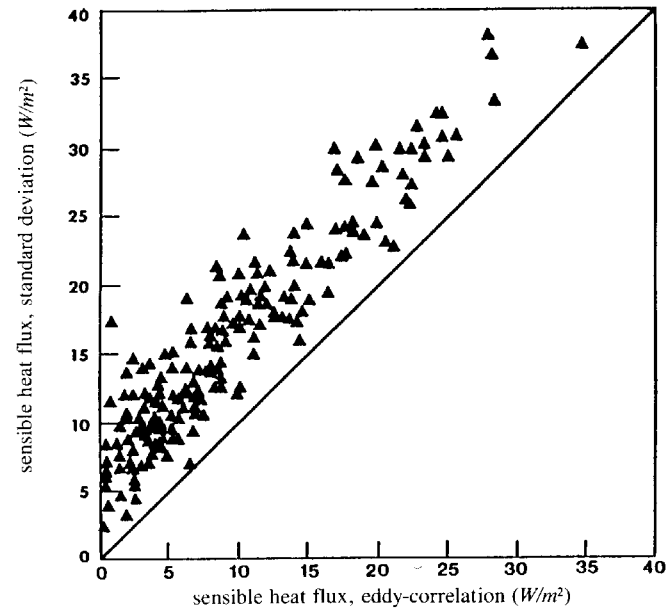

FIGURE 9.6. Nonuniform terrain. The sensible heat flux measured (eddy-correlation) at different locations and levels after the step change (locations 9, 8, and 10 in Fig. 9.4) compared with the sensible heat flux calculated with the variance technique [Equation (3)].

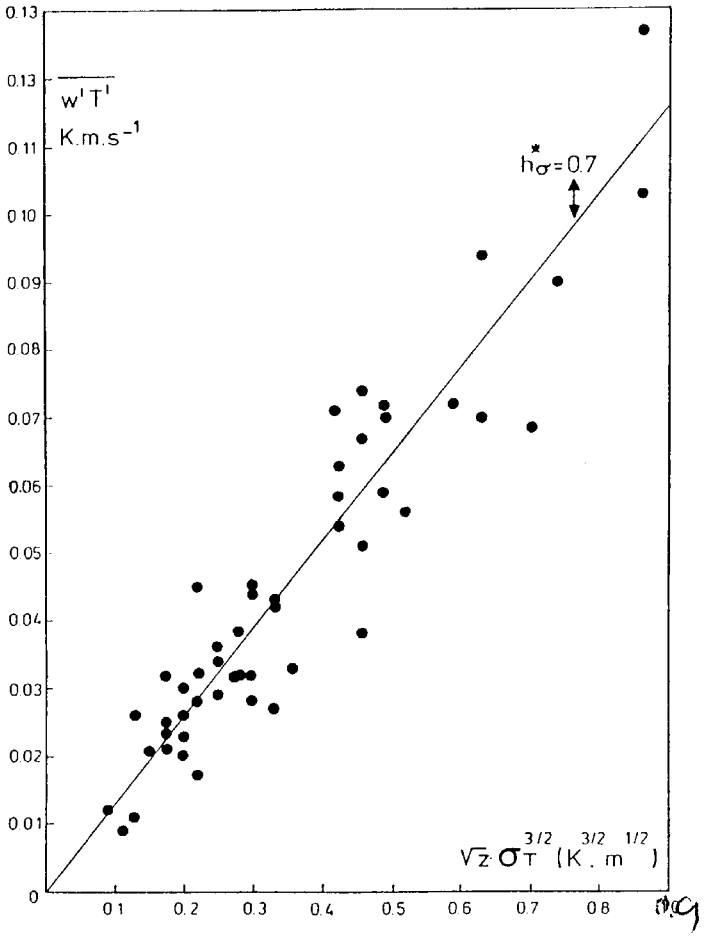

FIGURE 9.7. Nonuniform terrain at Cabauw. The sensible heat flux at z=22.5 m measured with the eddy-correlation method compared with the sensible heat flux derived from the variance technique [Equation (4) from de Bruin 1982]. Note that the axes differ from those in Figures 9.5 and 9.6 ($w'T'=u^*\theta^*$ versus $z^{1/2}\sigma_T^{3/2}$).

and the measured heat flux using an iterative procedure.

For the data selection the following criteria were used:

1. Only unstable conditions are considered, $z/L<0$.
2. Air had to be advected from the dry terrain to the wet terrain during a period of days with no rain. The range of wind directions of interest to us is indicated in Figure 9.4. Days with wind directions within this range are selected.

For a period of 5 consecutive days the wind direction was within this range. The angle of incidence of the flow at the leading edge was about 30° with a wind direction of 340° during the selected period, June 20 to 24, 1987. During that period the weather was fair with midday temperatures (measured in a Stevenson screen above the dry terrain) of 23°C on June 20 up to 28°C on June 24. The Mistral was blowing with 10 to 15 m/s at 10 m height. On June 19 there was some rain.

4. Results and Discussion

In Figures 9.5, 9.6, and 9.7 the observed (eddy-correlation) sensible heat flux density is plotted against the corresponding estimated values obtained with the variance method [Equation (3)] for three terrains: (1) the upwind dry field in the Crau, (2) the downwind irrigated field in the Crau, and (3) Cabauw, the Netherlands; respectively a uniform terrain, a nonuniform of type a and a nonuniform type b terrain (see Section 1). Figure 9.7, referring to the latter site, is taken from de Bruin (1982).

It can be clearly seen that the variance method yields good results for the uniform site as well as

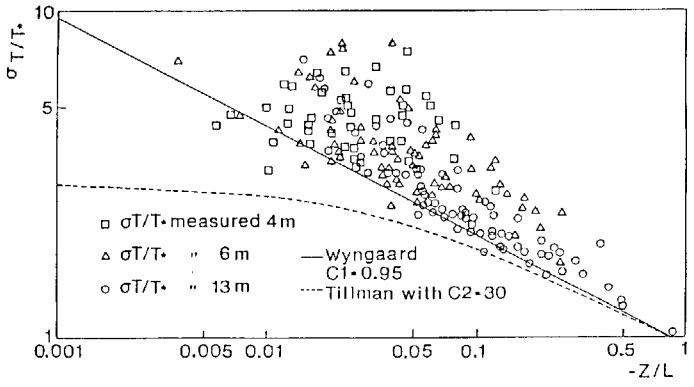

FIGURE 9.8. The measured σ_T/θ^* versus z/L compared with the free convection formulations of Wyngaard et al. (1971) and Tillman (1972) [Equations (5) and (3)].

for the terrain at Cabauw, which is nonuniform of type b. Over the irrigated field the variance method overestimates the sensible heat flux significantly under the present conditions.

This example shows that it makes sense to distinguish between type a and type b. In the first case the temperature and sensible heat flux are highly affected by the step-change in surface conditions, while in the second case only the wind speed and the momentum flux are influenced. Note that the flux-profile relationships found at Cabauw deviate significantly from those over uniform terrain (Beljaars et al., 1983).

In Figure 9.8 σ_T/θ_* is plotted versus the *local* value of z/L; these data were gathered over the irrigated field at a height of 4, 6, and 13 m. For comparison, the curves corresponding to Equation (9.2) (Tillman curve) and Equation (9.5) (free convection) are drawn. It is seen that almost all points lie above both curves. In Figure 9.8 we used the *local* values of z/L because the fluxes vary significantly with height (see later). It is questionable whether this local z/L is a suitable scaling parameter (Lang et al., 1983). This is yet an unsolved problem. Note that it is one of the objectives of this study to show the limitations of the M–O similarity theory in real applications. These limitations are clearly demonstrated in Figure 9.8.

A similar plot for water vapor, σ_q/q^* versus z/L, is presented in Figure 9.9. This can be done since it is expected that Equations (9.1) to (9.5) are valid for all scalars.

It appears that in this case the deviation from the Tillman curve is almost absent and falls within the experimental error. Apparently, the *local* water vapor flux scales with the *local* z/L similarly to the homogeneous case. Note that Figure 9.9 does not contain information of the surface evaporation, because the water vapor flux varies so much with height.

In Figure 9.10 some measured profiles of temperature and humidity for increasing distances from the step-change at midday are presented.

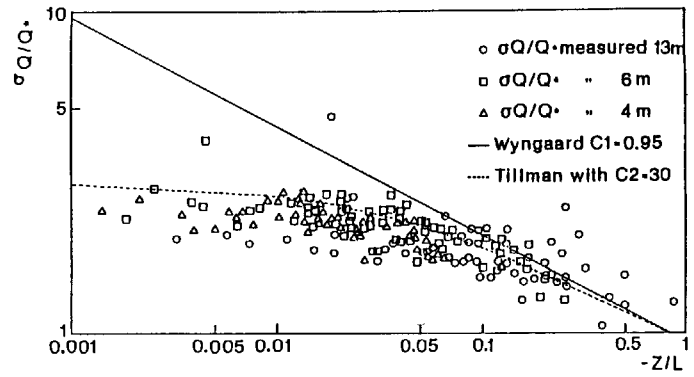

FIGURE 9.9. The measured σ_q/q^* versus z/L compared with the free convection formulation of Wyngaard et al. (1971) and Tillman (1972) [Equations (5) and (3), but for moisture].

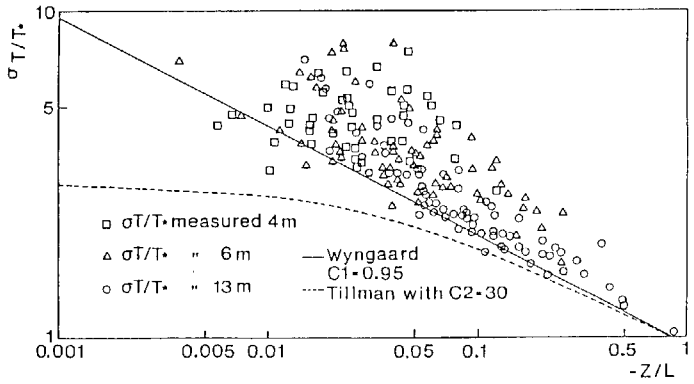

FIGURE 9.8. The measured σ_1/θ^* versus z/L compared with the free convection formulations of Wyngaard et al. (1971) and Tillman (1972) [Equations (5) and (3)].

for the terrain at Cabauw, which is nonuniform of type b. Over the irrigated field the variance method overestimates the sensible heat flux significantly under the present conditions.

This example shows that it makes sense to distinguish between type a and type b. In the first case the temperature and sensible heat flux are highly affected by the step-change in surface conditions, while in the second case only the wind speed and the momentum flux are influenced. Note that the flux-profile relationships found at Cabauw deviate significantly from those over uniform terrain (Beljaars et al., 1983).

In Figure 9.8 σ_T/θ_* is plotted versus the *local* value of z/L; these data were gathered over the irrigated field at a height of 4, 6, and 13 m. For comparison, the curves corresponding to Equation (9.2) (Tillman curve) and Equation (9.5) (free convection) are drawn. It is seen that almost all points lie above both curves. In Figure 9.8 we used the *local* values of z/L because the fluxes vary significantly with height (see later). It is questionable whether this local z/L is a suitable scaling parameter (Lang et al., 1983). This is yet an unsolved problem. Note that it is one of the objectives of this study to show the limitations of the M–O similarity theory in real applications. These limitations are clearly demonstrated in Figure 9.8.

A similar plot for water vapor, σ_q/q^* versus z/L, is presented in Figure 9.9. This can be done since it is expected that Equations (9.1) to (9.5) are valid for all scalars.

It appears that in this case the deviation from the Tillman curve is almost absent and falls within the experimental error. Apparently, the *local* water vapor flux scales with the *local* z/L similarly to the homogeneous case. Note that Figure 9.9 does not contain information of the surface evaporation, because the water vapor flux varies so much with height.

In Figure 9.10 some measured profiles of temperature and humidity for increasing distances from the step-change at midday are presented.

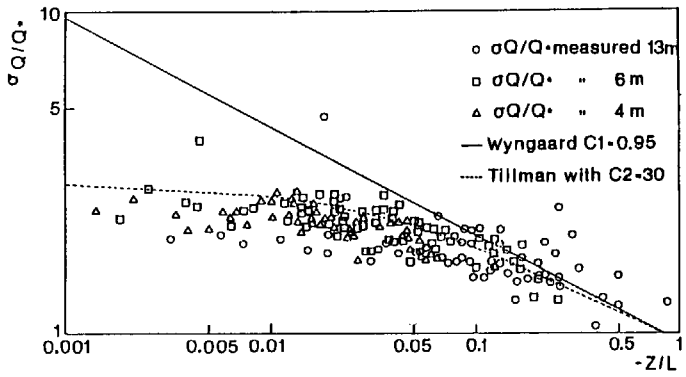

FIGURE 9.9. The measured σ_q/q^* versus z/L compared with the free convection formulation of Wyngaard et al. (1971) and Tillman (1972) [Equations (5) and (3), but for moisture].

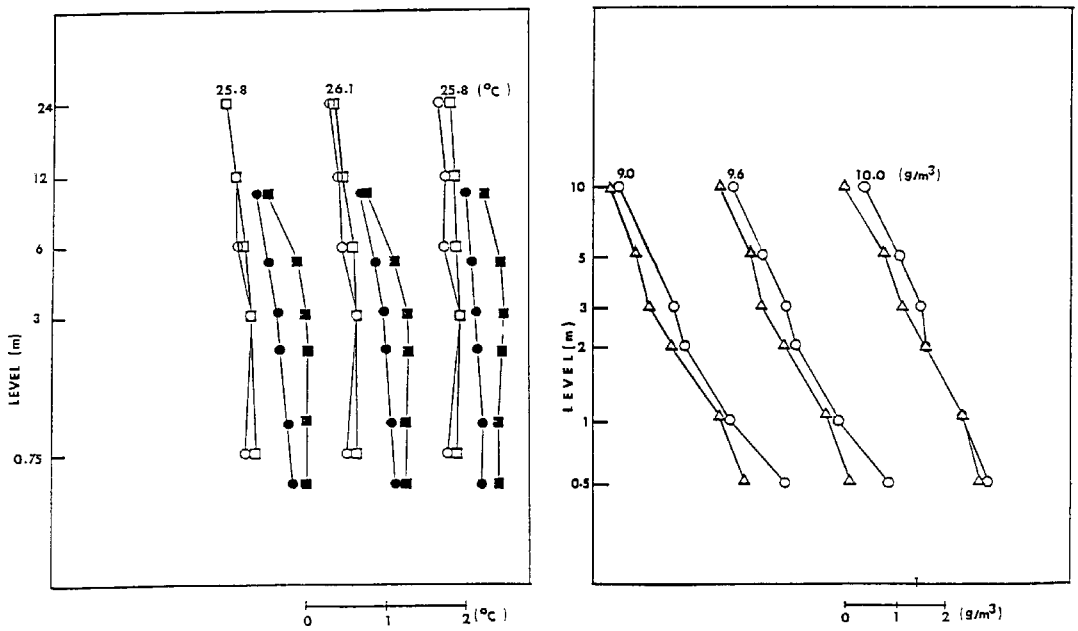

FIGURE 9.10. Profiles of temperature (80, 120, 150, and 200 m after the step) and for humidity (80 and 120 m after the step).

The temperatures measured at about 80 m from the step are the highest. Cooling of the air with distance from the step change is clearly observed. In the first 120 m the most rapid changes in the profile can be noticed where the IBL is still thin. At 150 m and 200 m the profiles show a so-called advective inversion (Lang et al., 1983).

The variation of the profiles in the horizontal direction is reflected in the local divergence of the fluxes with height. The latter is clearly shown in Figure 9.11, in which the observed flux densities of latent and sensible heat are depicted over, respectively, the dry terrain at 6 m height and for the 4, 6, and 13 m levels at almost the same distance from the step change over the irrigated field.

In Figure 9.12 a comparison is given between the calculated profiles of temperature and humidity at 80 m from the leading edge, using the second-order closure model of Rao et al. (1974) and the corresponding measured profiles. As noted before we included the Monteith's "big leaf" concept as lower boundary condition in this version of the model. We carried out the calculations for different values of the surface resistance r_s. It appears that for r_s = 30–45 s/m the observed profiles are reasonably described by the model. In a next study the calculated fluxes will be compared with the measured ones.

5. Concluding Remarks

This chapter deals with the surface fluxes of heat and water vapor near a nonuniform surface, in particular an irrigated field surrounded by dry terrain. A first analysis of data obtained from an extensive micrometeorological field experiment reveals that the fluxes can vary significantly with height and that (therefore) strong deviations from the Monin–Obukhov similarity theory can occur over nonuniform terrain.

Also, it is shown that it makes sense to distinguish between two types of nonuniform terrains:

1. Type a, where the temperature and humidity field are highly affected and the wind field is not, and
2. Type b, where the wind field is disturbed and the temperature and humidity field is not.

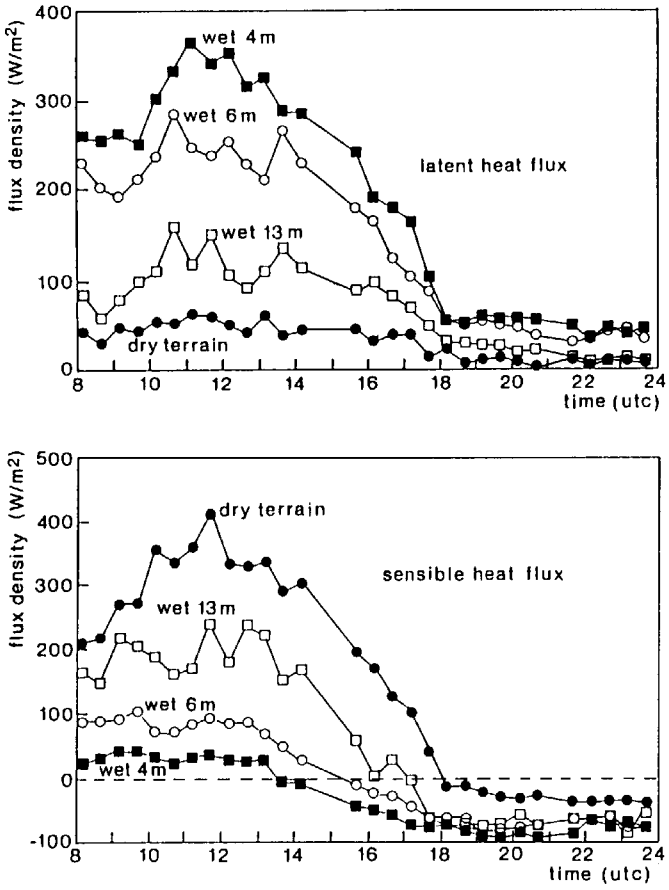

FIGURE 9.11. The flux densities for heat and water vapour at Crau, France, June 23, 1987, above the dry terrain and above the wet terrain at different levels (locations 4, 8, 9, and 10 in Fig. 9.4). Not corrected for distortion errors.

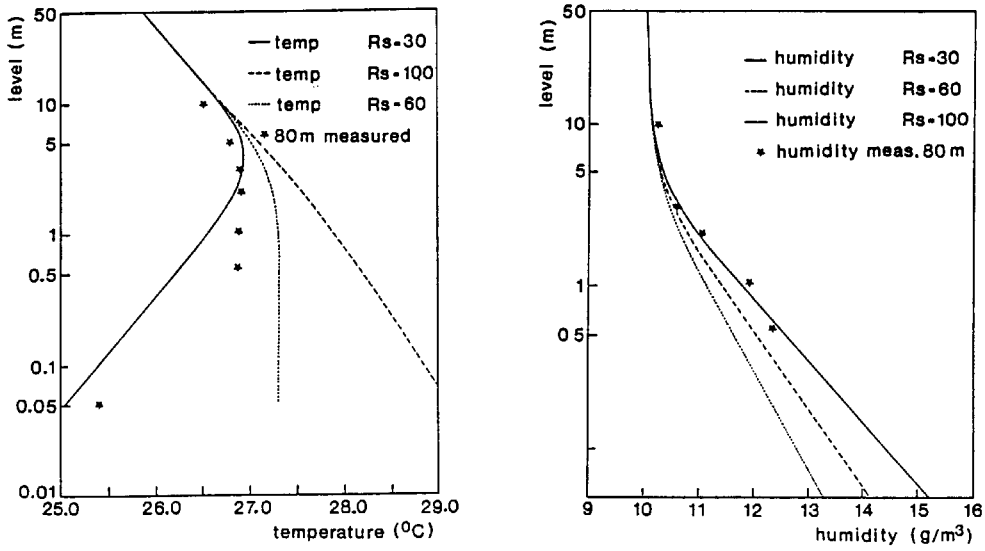

FIGURE 9.12. Model calculations and measurements of temperature and humidity profiles behind a dry-to-wet step change.

Evidence is presented that the variance method as used by Tillman (1972), by which fluxes can be obtained from simple single-level observations is still applicable over nonuniform fields of type b.

The first comparison between data and calculations done with the second-order closure model of Rao et al. (1974), in which we changed the surface boundary conditions by using the big-leaf concept of Monteith, is promising. It appears that the results depend critically on the surface resistance.

Acknowledgments. Mr. Py allowed us to use his farm and crop for the experiment. The data used in this paper were collected in close cooperation with Dr. H. F. Vugts, Dr. F. Cannemeijer, and F. Tesselaar from the Department of Meteorology of the Free University of Amsterdam. Dr. B. Sequin and Dr. F. Verbrugge from I.N.R.A, Avignon are acknowledged for their hospitality and support in France. Both the technical staffs of our institute and of the Free University of Amsterdam did indispensable work before and after the measuring period. The software for the data processing was skillfully developed by Dr. Ir. J. van Boxel. One of the authors, Ir. N. J. Bink, is supported by the Working Group on Meteorology and Physical Oceanography (MFO) with financial aid from the Dutch Organization for Scientific Research (NWO). This study is partly sponsored by the EC under contract number EV4C/0015NL. We are grateful for the valuable comments of Bart v.d. Hurk.

Appendix 1: List of Symbols

Symbols of quantities	Dimension	Description
a_1		Constant for the parameterization of the third order moments
b		Constant for the parameterization of ε_M
C_1		Constant in free convection scaling formulation of Wyngaard et al. (1971)
C_2		Constant in scaling formulation of Tillman (1972)
c		Constant for the parameterization of ε
c_p	J kg^{-1} K^{-1}	Specific heat of air at constant pressure
$d_{i=1,2,3}$		Constants for the parameterization of the pressure-gradient covariance term
g	m s^{-1}	Acceleration of gravity
H	W m^{-2}	Sensible heat flux density
k		von Karman constant, taken as 0.4
L	m	Monin–Obukhov length
p'	Pa	Pressure fluctuations
q'		Moisture fluctuations
q^*		Characteristic specific humidity
r_s	s m^{-1}	Surface resistance
$U_{i=1,2,3}$	m s^{-1}	Wind speed vector (U, V, W) in the x, y, z or x_1, x_2, x_3 directions
u^*	m s^{-1}	Friction velocity
$u'_{i1,2,3}$	m s^{-1}	Vector of the velocity fluctuations (u, v', w') in the x, y, z or x_1, x_2, x_3 directions
x	m	Horizontal distance along the wind direction
$x_{i1,2,3}$	m	Spatial coordinates x, y, and z
y	m	Horizontal distance perpendicular to the wind direction
z	m	Height
z_0	m	Surface roughness length
δ_{ij}	-	Kronecker's delta: if $i = j$ then $\delta = 1$, else $\delta = 0$
ε	m^2 s^{-3}	Rate of dissipation of the turbulent energy $\overline{u'_i u'_i}$ into heat
ε_M	m^2 s^{-3}	Rate at which $\overline{\theta'^2}$, $\overline{q'^2}$, or $\overline{\theta' q'}$ are smoothed out by molecular conduction
ρ	g/m^3	Air density
σ_s	(depends	Standard deviation of the quantity s
τ	s on s)	Turbulent relaxation time
θ	K	Potential temperature
θ'	K	Potential temperature fluctuations
$\theta_* = H/\rho\, c_p\, u^*)$	K	Characteristic potential temperature

Appendix 2: Second-Order Closure Modeling

The conservation equations of momentum, mass, specific entropy, and water vapor are used as a starting point for the derivation of the transport equations for various meteorological variables that will be affected by a change in surface conditions.

If the proper simplifying assumptions are used, and if the restriction is made of a flow at right angles to the surface discontinuity (a two-dimensional case), then it is possible to derive a set of transport equations for the mean quantities $U_i=(U, O, W)$, θ, and Q (see, e.g., Brutsaert, 1982; Kroon, 1985). The corresponding fluctuating components are indicated by $u'_i=(u', v', w')$. Note that repeated indices in one term denote summation (Einstein's convention).

By deriving the equations for the four mean quantities, additional unknowns are created, i.e., $\overline{u'w'}$, $\overline{w'\theta'}$, and $\overline{w'q'}$. Hence the four equations do not form a closed system, i.e., a system where the number of equations equals the number of unknowns. To close this system several solutions are proposed. In the second-order closure models a set of transport equations for the turbulence quantities is derived from the governing equations.

These transport equations, however, also contain a number of unknown variables (third-order terms, pressure terms etc.). In second-order closure models (e.g., Rao et al., 1974) the third-order and pressure terms are closed by expressing these quantities as a function of first- and second-order moments using (semi)empirical relations.

Generally speaking, second-order closure models contain three different higher order terms, which have to be parameterized to close the system of equations. These terms will be briefly discussed.

A2.1 Turbulent Transport Terms

These terms all have the form $\partial\overline{Mu'}/\partial x_j$, where M can be any second moment combination of u', w', θ', and q' (e.g., $\overline{u'q'}$). Using Gauss' integral theorem it is possible to show that these terms merely tend to redistribute the quantity M from one point inside the flow to another. In the model of Rao et al. (1974) a simple ad hoc gradient diffusion modeling of these terms is used viz.

$$\overline{Mu'_i} = a_t \frac{\partial M}{\partial x_j} \overline{u'_i u'_j} \tau \qquad \text{(A2.1)}$$

where a_t is a constant and τ is a turbulent relaxation time.

A2.2 Pressure Covariance Terms

In the equation of the Reynolds' stress $\overline{u'_i u'_k}$ the pressure covariance term reads

$$u'_k \frac{\partial p'}{\partial x_i} + u'_i \frac{\partial p'}{\partial x_k} \qquad \text{(A2.2)}$$

Analysis of homogeneous two-dimensional flows (e.g., Hinze, 1959) shows that this term redistributes the turbulent kinetic energy in that it forces the $(\overline{u'_i})^2$ distributions toward isotropy and destroys the off-diagonal components of the $\overline{u'_i u'_k}$ tensor.

A pressure term is also generated in the $\overline{u'_i\theta'}$ and $\overline{u'_i q'}$ transport equations. In Rao's model they are modeled as follows:

$$-\overline{M\frac{\partial p'}{\partial x_i}} = d_i \frac{\overline{Mu'_i}}{\tau} \qquad \text{(A2.3)}$$

where M is either q' or θ', and d_i is a constant.

No general agreement on the modeling of the pressure covariance terms exists. In Rao's model no buoyancy and mean strain effects are incorporated in the pressure covariance term. Expressions incorporating these effects were presented by Wyngaard (1975).

A.2.3 Dissipation Terms

The dissipation terms indicate the molecular action on the turbulent correlations. It appears that viscous dissipation is the major loss term for turbulent kinetic energy. It can be demonstrated that in a Newtonian fluid the dissipation terms only affect the variances $\overline{u'^2_i}$, $\overline{q'^2}$, $\overline{\theta' q'}$. The off-diagonal elements of the Reynolds stress tensor $\overline{u'_i u'_k}$ as well as the turbulent fluxes $\overline{u'_i\theta'}$ and $\overline{u'_i q'}$ are not affected. In Rao's model the dissipation terms were modeled by

$$\varepsilon = c \frac{\overline{u'_i u'_k}}{\tau} \delta_{ik} \qquad \text{(A2.4)}$$

$$\varepsilon_M = b\frac{M}{\tau} \qquad \text{(A2.5)}$$

where δ_{ik} is Kronecker's delta ($\delta = 1$ if the indices are equal else $\delta = 0$), M is either $\overline{\theta'^2}$, $\overline{q'^2}$, or $\overline{\theta' q'}$, and c and b are constants.

References

Beljaars ACM, Schotanus P, Nieuwstadt FTM (1983) Surface layer similarity under non-uniform fetch conditions. J Climatol Appl Meteorol 22:1800–1810.

Bruin HAR de (1982) The energy balance of the Earth's surface. Ph.D. dissertation, Agricultural University, Wageningen.

Brutsaert WH (1982) Evaporation into the atmosphere. "Environmental Fluid Mechanics." D. Reidel, Dordrecht, Holland.

Hinze JO (1959) "Turbulence." McGraw-Hill, New York.

Kroon LJM (1985) Profile derived fluxes above inhomogeneous terrain: A numerical approach. Ph.D. dissertation, Agricultural University, Wageningen.

Lang ARG, McNaughton KG, Fazu C, Bradley EF, Othaki E (1983) Inequality of eddy tranfer coefficients for vertical transports of sensible heat and latent heat under advective inversions. Bound Layer Meteorol 25:25–41.

McBean GA, Miyake M (1972) Turbulent transfer mechanisms in the atmospheric surface layer. Quart J R Meteorol Soc 98:383–398.

Monteith JL (1981) Evaporation and surface temperature. Quart J R Meteorol Soc 107:1–27.

Panofsky HA, Dutton JA (1984) "Atmospheric Turbulence, Models and Methods for Engineering Applications." Wiley, New York.

Rao KS, Wyngaard JS, Coté OR (1974) Local advection of momentum, heat and moisture in micrometeorology. Bound Layer Meteorol 7:331–348.

Schotanus P Nieuwstadt FTM, Bruin HAR de (1983) Temperature measurement with a sonic anemometer and its application to heat and moisture fluxes. Bound Layer Meteorol 26:81–93.

Tillman JE (1972) The indirect determination of stability, heat and momentum fluxes in the atmospheric boundary layer from simple scalar variables during dry unstable conditions. J Appl Meteorol 11:783–792.

Vugts HF, Cannemeijer F, Tesselaar F (1988) The Crau experiment. Parameterization of the surface fluxes. Internal report Free University Amsterdam, Department of Meteorology.

Wyngaard JC (1975) Modelling the planetary boundary layer-extension to the stable case. Bound Layer Meteorol 9:441–460.

Wyngaard JC, Coté OR, Izumi Y (1971) Local free convection, similarity, and the budgets of shear stress and heat flux. J Atmos Sci 28:1171–1182.